Garcers, G.; Requena, G.; Tolnai, D.; Perez, P.; Adeva, P.; Stark, A.; Schell, N.:
Influence of rare-earth addition on the long-period stacking ordered phase in cast Mg–Y–Zn alloys
In: Journal of Materials Science (2014) Springer

DOI: 10.1007/s10853-013-7967-4

Influence of Rare-earth addition on the Long-Period Stacking Ordered phase in cast Mg-Y-Zn alloys

Gerardo Garcés[a,*], Guillermo Requena[b], Domonkos Tolnai[c], Pablo Pérez[a], Paloma Adeva[a], Andreas Stark[c], Norbert Schell[d].

a) DepartmentofPhysical Metallurgy, NationalCenter for Metallurgical Research (CENIM-CSIC), Avda. Gregorio del Amo 8, 28040 Madrid, Spain
b) Institute of Materials Science and Technology,ViennaUniversity of Technology, Karlsplatz 13/308, A-1040 Vienna, Austria
c) Institute of Materials Research, Helmholtz-ZentrumGeesthacht, Max-Planck-Str. 1, 21502 Geesthacht, Germany
d) Structural Research on New Materials, Helmholtz-ZentrumGeesthacht Outstation at DESY in Hamburg, Germany

Abstract

The microstructure and thermal stability of the $Mg_{97}Y_2Zn_1$(at.%) alloy, modified with the addition of 0.5 at.% of gadolinium or neodymium, have been examined by synchrotron radiation diffraction during in-situ differential scanning calorimetry. The microstructure of the three alloys consists of magnesium dendrites with the *Long Period Stacking Ordered* (LPSO) phase at interdendritic regions. Rare-earth atoms substitute yttrium atoms in the LPSO phase, promoting the formation of the 14H structure. Lattice parameters of the LPSO do not change significantly with the rare earth addition. However, they reduce the melting point of the LPSOphase, especially in the case of neodymium addition.

Keywords: Magnesium alloys; LPSO; Synchrotron diffraction.

*corresponding author: Tel.: +34915538900; fax: +34-915347425
E-mail address: ggarces@cenim.csic.es (Gerardo Garcés)

1. Introduction

Magnesium alloys combining yttrium/rare earth (Y, Gd, Nd, Dy, etc) elements and transition metals (Zn, Cu, Ni) are effectively strengthened by the presence of *Long Period Stacking Ordered* (LPSO) structures [1-8]. They can combine high strength with acceptable ductility and enhanced creep resistance. LPSO-phases are solid solutions of yttrium or rare-earthelements and transition metals in the magnesium lattice, where these atoms are arranged periodically in the magnesium basal planes forming ordered structures [9-12]. *Different LPSO crystal structures have been reported, i.e., 6H, 10H, 14H, 18R and 24R [13-15] depending on the thermal history of the material. The 18R structure is observed mainly in the as-cast condition. However, this structure is not stable at high temperature and is gradually replaced by a 14 H structure[11]. Recently, Egusa and Abe[12] have proposed crystal/order structural models for 18R and 14H phases formed in Mg–Zn–RE alloys. These phases can be rationalized by space groupsC2/m, $P3_112$ or $P3_212$ for the 18R type and P63/mcm for the 14H type. The characteristic ordered features are well represented by local Zn_6RE_8 clusters, which are embedded in the fcc stacking layers in accordance with the $L1_2$ type short-range order.*

A $Mg_{97}Y_2Zn_1$(at.%) alloy produced by warm extrusion of rapid solidified ribbons exhibited high yield strength, about 610 MPa, with 5% of elongation at room temperature[1]. Recently, Yamasaki et al.[4] have developed extruded $Mg_{97}Y_2Zn_1$(at.%) alloys that combine high yield stress (around 350 MPa) and acceptable ductility (around 8%) by controlling the cooling rate during the casting process and the extrusion parameters.

Optimization of the microstructure by developing fine lamella inside the magnesium grains can be achieved through an appropriate thermal treatment, resulting in additional

strengthening[8,16,17]. At room temperature, the hardening induced by these long plates is small. This fact is attributed to the crystallographic orientation of the precipitates within the magnesium matrix. Since they are located in basal planes, they have a low hardening effect on the basal slip system[18]. However, at high temperature, where non-basal slip systems are active, the lamellar structure increases the creep resistance of these alloys [8]. *In a recent review about precipitation and hardening in magnesium alloys[19], Nie concluded that precipitate plates formed on prismatic planes provide the most effective barrier to gliding dislocations and propagating twins in the magnesium matrix. The formation of this kind of precipitates has been reported in Mg-Y-RE systems, such a Mg-Y-Nd, Mg-Gd, Mg-Gd-Nd, etc. Moreover, Nie suggested that a higher strength can be achieved if a high density of strong plate-shaped precipitates with prismatic and basal habit planes and with a high aspect ratio can be introduced. Recently, it has been reported that the addition of rare-earth elements to the Mg-Y-Zn system containing LPSO phases promote the formation of plates in the prismatic and basal planes, preserving the LPSO phase in some conditions, and considerably increasing the strength of Mg-Y-RE-Zn(RE=Gd and Nd) alloys at room temperature[20-22]*.

The presence of additional elements can modify the crystallography and thermal stability of the LPSO phase. Therefore, this paper explores the influence of the additionof 0.5 at.% of Gd and 0.5 at.% of Nd to the $Mg_{97}Y_2Zn_1$(at.%) alloy.

2. Experimental procedure

Three alloyswith nominal compositions $Mg_{97}Y_2Zn_1$(at.%), $Mg_{96.5}Y_2Zn_1Gd_{0.5}$(at.%) and $Mg_{96.5}Y_2Zn_1Nd_{0.5}$(at.%) were prepared by melting high purity elements Mg and Zn and Mg-22%Y(wt.%), Mg-20%Gd(wt.%) and Mg-22%Nd (wt.%) master alloys in an

electric resistance furnace. The three alloys were cast in a 12 mm diameter cylindrical steel mould. For comparative purposes, a fully LPSO alloy with composition $Mg_{88}Y_8Zn_4$(at.%) was also prepared in an induction melting furnace using a graphite tube coated with boron nitride in argon atmosphere. The fully LPSO alloy was homogenized at 350 ºC for 24 hours.

Microstructural characterization of the alloys was carried out by optical (OM), scanning (SEM) and transmission electron microscopy (TEM). Specimens for TEM observation were prepared by electrolytic polishing using a reactive mixture of 25% nitric acid and 75 % methanol at -20ºC and 20V. Then, ion milling at liquid nitrogen temperature was used to remove the fine oxide film formed on the surface during electrolytic polishing.

The thermal stability of the three alloys was monitored by DSC experiments using heating/cooling rates of 10 $Kmin^{-1}$ under argon atmosphere in a Mettler Toledo 822 DSC equipment. The samples were subjected to one DSC heating/cooling cycle between RT and 570 °C.

Synchrotron radiation diffraction was performed at the P07 – HEMS beamline of PETRA III, at the DeutschesElektronen-Synchrotron (DESY) during in-situ DSC experiments. The samples were encapsulated in stainless steel crucibles during the measurement, using an empty crucible as reference. The DSC unit was placed inside the coil of a Bähr 805A/D dilatometer. The dilatometer and the DSC unit are modified for synchrotron experiments. Two Kapton windows on the sides of the chamber and a hole in the DSC pan allow the high energy X-ray beam to reach the sample and the detector without disturbance. The measurements were performed in argon flow. The diffraction patterns were recorded using an exposure time of 1 s by a Perkin-Elmer XRD 1622 flatpanel detector with an array of 2048^2pixel, with an effective pixel size of 200×200 μm^2. The beam energy was 100 keV, corresponding to a wavelength of 0.0124 nm.

LaB_6 was used as a reference to calibrate the acquired diffraction spectra. The detector-to-sample distance was 1918.95 mm. Conventional line profiles were obtained by azimuthal integration of the Debye-Scherrer rings. The heating/cooling rate of the DSC was 40 $Kmin^{-1}$ and 10 $Kmin^{-1}$ below and above 400 ºC, respectively. Similarly to the laboratory DSC scans, the samples were subjected to one DSC cycle between RT and 560 °C.

3. Results and Discussion

Figure 1(a-c) shows the microstructure of the $MgY_2Zn_1(RE_{0.5})$ alloys in the as-cast condition. The microstructure consists of magnesium dendrites with the LPSO phase distributed at interdendritic regions. The volume fraction of LPSO phase is similar for the three alloys, about 22 vol.%. The $Mg_{88}Y_8Zn_4$(at.%) alloy consists of long LPSO laths with a small volume fraction of magnesium islands (Figure 1d).

Figure 2 (a-h) shows the Debye-Scherrer rings obtained at RT for the alloys in the as-cast condition. It is interesting to note that diffuse scattering (streaking) is observed in the case of the LPSO phase in the $MgY_2Zn_1(RE_{0.5})$ alloys. This is especially marked for the smaller diffraction ring that correspondsto (0003) reflex of the 18R LPSO phase. Okuda et al.[*23*], using SAXS, reported diffuse streaks connecting diffracted spots suggesting that 18R and 10H structures coexist in a coherent way in the same grains. However, in this case, these diffuse streaks are not observed connecting reflexes from other LPSO structures. On the other hand, similar diffuse streaking has been observed in diffraction patternsby TEM. Li et al.[*24*] showed diffuse streaking in the [0001] direction due to the formation of stacking faults (SFs)in the (0001) basal plane of deformed pure magnesium. Garces et al.[8] also observed diffuse streaking along the [0002] direction in the magnesium grains of MgY_2Zn_1 alloys heat treated at high

temperature. This diffuse streaking was related tostacking faults in the basal plane due to the formation of long LPSO precipitates having the 14H structure. The fact that the streaking is radial to the diffraction ring indicates that the SFs are located parallel to the (0003) planes, namely in the *c* direction of the 18R LPSO lattice.

The integration of the Debye-Scherrer rings to obtain the diffraction patterns as a function of 2θ has been carried out using the software Fit2D[25]. As an example, Figure 3 shows the indexed Debye-Scherrer rings and the 2θ diffraction patterns for the MgY_2Zn_1 alloy. Figure 4 shows the integrated diffraction patterns obtained at room temperature for the four alloys in the as-cast condition together with the theoretical diffraction reflections of Mg and those of the 18R and 14H LPSO phase. The diffraction pattern of the 18R and 14H crystal structures were simulated using Carine 3.1*[26]* according to the structure described in[12]. The 18R type and 14H type crystal structures belong to the space groups $P3_212$ and $P6_3/mcm$, respectively. It can be seen that the crystal structure of the LPSO phase in the four as-cast alloys corresponds mainly to the 18R structure.

Lattice parameters of LPSO and magnesium phases can be calculated from the diffraction patterns of *Figure 4*. In all studied alloys, the use of a Rietveld fit is difficult due to the large overlapping exhibited by several reflexes of Mg and LPSO structures. Therefore, isolated peaks from each phase have been individually fitted using the software PeakFit*[27]*. Table 1 shows *a* and *c* values for the LPSO and magnesium phases, respectively. The lattice parameters of the LPSO phase are similar in all the cases and are in agreement with the literature[12]. The fitting errors in $MgY_2Zn_1(RE_{0.5})$ alloys are larger than for the MgY_8Zn_4 alloy because the intensity of diffracted peaks corresponding to the LPSO phase is smaller and the diffracted peaks are broader due to the diffusive scattering (Figure 2 e-g). The lattice parameter *a* of Mg shows an increase

with respect to pure Mg (a = 0.32089 nm and c = 0.52101 nm*[28]*). The magnesium phase in the $MgY_2Zn_1(RE_{0.5})$ alloys contains a small amount of yttrium in solid solution which is reported to increase *a*, i.e. reducing the *c/a* ratio*[29,30]*.

As described above, the diffuse scattering results in a very broad (0003) diffraction peak of the 18R structure, located at 2θ = 0.44º. Furthermore, overlapping with a second peak at smaller angles seems to take, especially for the $Mg_{97}Y_2Zn_1Nd_{0.5}$ alloy. This may indicate the coexistence of 18R and 14H LPSO in the as-cast alloys. *Figure 5a* shows a detail of the lamellar structure corresponding to the LPSO phase in the as-cast $Mg_{97}Y_2Zn_1Nd_{0.5}$ alloy. The contrast variation in the SEM image can be related to composition or crystallographic heterogeneities. *Figure 5b provides a two-beam bright-field image for the LPSO phase using g = 0002$_\alpha$ diffraction vector in the* $\langle 11\bar{2}0\rangle_\alpha$ *zone axis in the $Mg_{97}Y_2Zn_1Nd_{0.5}$ alloy.* The18R and 14H crystal structures can be identified through the selected area electron diffraction pattern (SAED) in the $\langle 11\bar{2}0\rangle_\alpha$ zone axis or by measuring the fringe spacing in the $[0002]_\alpha$ direction formed when the **g** = 0002 is excited. The coexistence of 18R and 14H structures with a fringe spacing of about 1.6 and 1.8 nm, respectively, can be observed. This fact can be also observed in the SAED in the $\langle 11\bar{2}0\rangle_\alpha$ *zone axis where the diffracted spots of both structures are overlapped. Moreover, the SAED pattern shows weak streaks along [0001] direction and are visible through the ±1/2{1100} positions. Zhu et al.[11] indicated that the presence of these weak streaks provides important information on the ordered arrangement of Y and Zn in the 18R and 14H structures.*

Table 2 shows the composition of the LPSO phase determined by energy dispersive spectroscopy (EDS) for the three $MgY_2Zn_1(RE_{0.5})$ alloys in the as-cast condition and after the DSC scan. The composition of the LPSO phase in the $Mg_{97}Y_2Zn_1$(at.%) alloy is similar to that reported in a previous study[11]. Gadolinium and neodymium

additions have two different effects on LPSO phase composition. On one hand, zinc content slightly decreases with respect to LPSO formed in the $Mg_{97}Y_2Zn_1$ alloy. On the other hand, yttrium content decreases up to approximately 5 at.%, while the rare-earth content is around 1.5 at.% in both alloys in as-cast condition. The sum of yttrium and rare earth concentration in quaternary alloys is equal to the yttrium content in the ternary alloy, indicating that rare-earth atoms substitute yttrium atoms in the LPSO structure. Thus, an increase in the volume fraction of the LPSO phase in the $Mg_{97}Y_2Zn_1Gd_{0.5}$ and $Mg_{97}Y_2Zn_1Nd_{0.5}$ alloys may be expected due to the excess of yttrium. However, the volume fraction of the LPSO phase is similar in the three alloys (about 22 vol%) suggesting that the maximum volume fraction of the LPSO phase in the alloys is fixed by the zinc content. Therefore, the excess of yttrium and rare earth elements could favour the formation of new phases.

Figure 6 shows laboratory DSC scans during heating and cooling for the three $Mg_{97}Y_2Zn_1(RE)_{0.5}$ alloys. *It is important to note that the use of the term "laboratory" is used to distinguish from the DSC scans obtained in the in-situ experiments.* An endothermic peak is observed during heating and one or two exothermic peaks during cooling depending on the alloy. The endothermic and exothermic reactionsare displaced to lower temperatures with the additions of rare earth elements. Neodymium results in a larger temperature displacement than gadolinium. During heating, the rare-earth-containing alloys show only one endothermic reaction, but two clear exothermic peaks can be observed during cooling. The separation between the exothermic reactions is larger for the alloy with Nd than for that with Gd addition. *Figure 7a* shows synchrotron diffraction patterns for the $Mg_{97}Y_2Zn_1$(at.%) alloy at 400 ºC during heating, at 560 ºC (the temperature at the end of the endothermic peak) and at 400 ºC during cooling. At 400 ºC during heating, reflections corresponding to the magnesium matrix, the LPSO

phase with the 18R crystal structure and the stainless steel pan (SP) are observed. At 560 ºC, right after the endothermic peak, the reflections of the 18R crystal structure disappear, remaining exclusively reflections from the magnesium phase and the steel pan. At 400 ºC, during cooling, diffraction peaks corresponding to the LPSO phase reappear, but now with coexisting 18R and 14H structures. This indicates that the endothermic and exothermic reactions are related to melting and solidification of the LPSO phase, respectively. The addition of the rare-earth elements decreases the melting point of the LPSO phase, as it is evidenced in *Figure 6* by the displacement of the endothermic peaks of the $Mg_{97}Y_2Zn_1Gd_{0.5}$ and $Mg_{97}Y_2Zn_1Nd_{0.5}$ alloys to lower temperatures in comparison with the $Mg_{97}Y_2Zn_1$ alloy. Since the melting points of yttrium, gadolinium and neodymium are 1526, 1311 and 1010 ºC*[28]*, respectively, the highest melting point for the LPSO phase should be expected for the $Mg_{97}Y_2Zn_1$, followed by the Gd-containing and Nd-containing alloys, as observed in DSC scans. This agrees with the experimental data (end temperature of the endothermic peak: 561 ºC, 556 ºC and 542 ºC for $Mg_{97}Y_2Zn_1$, $Mg_{97}Y_2Zn_1Gd_{0.5}$ and $Mg_{97}Y_2Zn_1Nd_{0.5}$, respectively).

Figure 7b shows the synchrotron diffraction patterns at 400 ºC during heating, at the highest temperature above the endothermic peak and at 400 ºC during cooling for the fouralloys in the 2θ range of 0.2-0.75º. In this 2θ range the diffraction peaks of the 18R and 14H crystallographic structures do not overlap considerably. The 18R structure is exclusively present in the alloys in as-cast condition since the cooling rate during casting was sufficiently fast to prevent formation of 14H structure[11]. However, while 18R and 14H structures coexist after the exothermic reaction during cooling in the three $MgY_2Zn_1(RE)_{0.5}$ alloys, the fully LPSO alloy only shows the 18R structure. The presence of the rare earth in solid solution in the LPSO phase has a strong influence in

its crystal structure during its formation in the course of solidification. *Figure 8* shows the diffraction patterns at low diffraction angle for the four studied alloys during cooling at the initial stage of the solidification of the LPSO phase. It must be pointed out that there is a difference of about +15 °C between the laboratory DSC and the in situ synchrotron diffraction experiments. This may arise due to the position of the thermocouple in the DSC unit of the Bähr dilatometer. This difference provokes a displacement of the temperature at which the reactions are measured but it does not influence the results. The temperature measured with the laboratory DSC equipment is more reliable and it must be considered as the correct one. Synchrotron diffraction data demonstrates that the 18R structure is formed first and then followed by the 14H one in the case of the MgY_2Zn_1 and $MgY_2Zn_1Gd_{0.5}$ alloys. However, in the $MgY_2Zn_1Nd_{0.5}$alloy, the 14H structure is rapidly developed and the intensity of the diffracted peak is even higher than that of the 18R structure.This is in agreement with the microstructure found in the as-cast condition, where the 14H structure is formed during solidification (*Figure 4 and 5*). These results indicate that the exothermic peak during cooling corresponds in fact to the overlapping formation of the 14H and 18R structures. However, the 18R structure is unstable and transforms into the 14H structure during heat treatments above 400 ºC[11]. Therefore, the 14H structure can be expected for sufficiently slow cooling rates. However, recent work by Grobner et al.*[31]*, which examine a phase diagram for LPSO and related phases in the Mg-rich corner of the ternary alloys, suggests a stable region in which 18R and 14H structures can coexist, as observed in this study. It is interesting to point out that in the case of the fully LPSO alloy, no 14H structure has been observed after cooling in the present work. The formation of 14H structure has been reported in the same alloy during a thermal treatment of 525 ºC during 3 days*[32]*. Since transformation from 18R to 14H structures

is slow, it is expected that lower cooling rates are required to observe the appearance of the diffracted peaks corresponding to the 14H structure in the fully LPSO alloy.

Figure 9 shows the microstructure of the $Mg_{97}Y_2Zn_1Nd_{0.5}$ alloy after the DSC scan. In the three alloys, the microstructure consists of magnesium and LPSO phases. The formation of a lamellar structure within the magnesium matrix is also found, identical to that reported previously in the $Mg_{97}Y_2Zn_1$ alloy[8,*16-17*,*33*]. The chemical composition of the LPSO phase determined by EDS after the DSC scan is very close to that in as-cast condition for the $Mg_{97}Y_2Zn_1$ and $Mg_{97}Y_2Zn_1Gd_{0.5}$ alloys (see Table 2). However, the Nd content in the LPSO phase in the $Mg_{97}Y_2Zn_1Nd_{0.5}$ alloy falls almost 50 %. Moreover, a new quaternary intermetallicphase has formed during cooling. This phase appears at lower temperatures than the LPSO phase as evidenced by the last exothermic peak at about 505 ºC for the $Mg_{97}Y_2Zn_1Nd_{0.5}$ alloy in *Figure 6*. Its composition is also listed in Table 2. The crystallography of this new phase is now under research. It has been reported that the LPSO phase forms in $Mg_{97}RE_2Zn_1$ alloys when yttrium and gadolinium are added but not in the case of Nd[5]. Therefore, the amount of neodymium dissolved in the LPSO phase is lower, 0.8 at.% , than that of gadolinium. The excess of neodymium is free to promote the formation of the new intermetallic phase found in this work.

4. Conclusions

The effect of the addition of 0.5 at.% of RE (Gd and Nd) on the microstructure and thermal stability of the LPSO phase in a $Mg_{97}Y_2Zn_1$(at.%) alloy has been studied. The microstructure of the as-cast alloy does not change significantly with the addition of Nd or Gd and consists of magnesium dendrites with the 18R LPSO phase distributed at interdendritic regions. RE atoms substitute yttrium atoms in the LPSO phase in the as-

cast condition and modified the crystallography of the LPSO phase, especially in the case of the addition of Nd which promotes the formation the 14H structure. Moreover, in this alloy, the LPSO phase is not stable and a new intermetallic phase is formed after the 14H and 18R LPSO phases during cooling from 570 °C at 10 Kmin^{-1}.RE addition decreases the melting point of the LPSO phase. The lower the melting point of the RE the lower the melting point of the LPSO phase.

Acknowledgements

The authors are grateful to MEC for financial support for this work under project MAT2009-07811. The DeutchesElektronen-Synchrotron DESY is acknowledged for the provision of beamtime at the P07 beamline of the Petra III synchrotron facilityin the framework of proposal I-20120285 EC.The authors would like to thank Dr. A. Rhys Williams for proof-reading the manuscript.

5. References

[1] Inoue A, Kawamura Y, Matsushita M, Hayashi K, Koike J (2001) Novel hexagonal structure and ultrahigh strength of magnesium solid solution in the Mg–Zn–Y system, J Mater Res 16:1894-1900.

[2] Kawamura Y, Kasahara T, Izumi S, Yamasaki M (2006) Elevated Temperature Mg97Y2Cu1 Alloy with Long Period Ordered Structure, ScrMater 55:453-456

[3] Hagihara K, Kinoshita A, Sugino Y, Yamasaki M, Kawamura Y, Yasuda HY, UmakoshiY (2010) Effect of long-period stacking ordered phase on mechanical properties of Mg97Zn1Y2 extruded alloy, Acta Mater58:6282-6293

[4] Yamasaki M, Hashimoto K, Hagihara K, Kawamura Y (2011) Effect of Multimodal Microstructure Evolution on Mechanical Properties of Mg-Zn-Y Extruded Alloy, Acta Mater 59:3646-3658.

[5] Kawamura Y, Yamasaki M (2007)Formation and Mechanical Properties of Mg97Zn1RE2 Alloys with Long Period Stacking Ordered Structure, MatTrans 48:2986-2992

[6] Garces G, Pérez P, Gonzalez S, Adeva P(2006) Development of Long-Period ordered structures during crystallization of amorphous $Mg_{80}TM_{10}Y_{10}$, Int J Mater Res 4:404-408

[7] Mi SB, Jin QQ (2013) New polytypes of long-period stacking ordered structures in Mg–Co–Y, Scripta Mater 68:635-638

[8] GarcesG, Oñorbe E, DobesF, PérezP, Antoranz JM, AdevaP (2012) Effect of microstructure on creep behaviour of cast $Mg_{97}Y_2Zn_1$ (at.%) alloy, MaterSci Eng A 539:48-55

[9] Luo ZP, Zhang SQ (2000) High-resolution electron microscopy on the X-Mg12ZnY phase in a high strength Mg-Zn-Zr-Y magnesium alloy, J Mater SciLetter 19:813-816

[10] Abe E,Kawamura Y, Hayashi K, Inoue A (2002)Long-period ordered structure in a high-strength nanocrystalline Mg-1 at% Zn-2 at% Y alloy studied by atomic-resolution Z-contrast STEM , Acta Mater50:3845-3857

[11] Zhu YM, Morton AJ, Nie JF (2010) The 18R and 14H long-period stacking ordered structures in Mg–Y–Zn alloys,Acta Mater 58:2936-2947

[12] Egusa D. Abe E (2012) The structure of long period stacking/order Mg–Zn–RE phases with extended non-stoichiometry ranges,Acta Mater 60:166-178

[13] Chino Y, Mabuchi M, Hagiwara S, Iwasaki H, Yamamoto A, Tsubakino H (2004) Novel equilibrium two phase Mg alloy with long-period ordered structure Scr Mater 51:771-714

[14] Matsuda M, Ii S, Kawamura Y, Ikuhara Y, Nishida M (2005) Variation of long-period stacking order structures in rapidly solidified Mg97Zn1Y2 alloy Mater Sci Eng A 393:269-274.

[15] Abe E, Ono A, Itoi T, Yamasaki M, Kawamura Y (2011) Polytypes of long-period stacking structures synchronized with chemical order in a dilute Mg-Zn-Y alloy Phil Mag. Letters 91:690-696

[*16*] Nie JF, Oh-ishi K, Gao X, Hono K(2008) Solute segregation and precipitation in a creep-resistant Mg–Gd–Zn alloy,Acta Mater 56:6061-6076

[*17*] Yamasaki M, Sasaki M, Nishijima M, Hiraga K, Kawamura Y (2007)Formation of 14H long period stacking ordered structure and profuse stacking faults in Mg-Zn-Gd alloys during isothermal aging at high temperature, Acta Mater 55:6798-680

[*18*] GengJ, ChunYB, StanfordN, DaviesCHJ, NieJF, BarnettMR(2011) Processing and properties of Mg–6Gd–1Zn–0.6Zr: Part 2. Mechanical properties and particle twin interactions, Mat Sci Eng A 528A:3659-3665

[19] Nie JF (2012) Precipitation and Hardening in Magnesium Alloys Met Mater Trans A 43:3891-3939

[*20*] Honma T, Ohkubo T, Kamado S,Hono K (2007) Effect of Zn additions on the age-hardening of Mg–2.0Gd–1.2Y–0.2Zr alloys,Acta Mater 55:4137-4150

[*21*] YinDD, WangQD, GaoY, ChenCJ, Zheng J(2011) Effects of heat treatments on microstructure and mechanical properties of Mg–11Y–5Gd–2Zn–0.5Zr (wt.%),J Alloys Comp 509:1696-1704

[*22*] LeeJB, K Sato, TJ Konno, Hiraga K (2011)Complex precipitates with long periodic stacking (LPS) phase and precipitation behaviors in the $Mg_{97}Zn_1Y_{1.5}Nd_{0.5}$ alloy by age-annealing , Intermetallics 19:1096-1101

[*23*] Okuda H, Horiuchi T, Tsukamoto T, Ochiai S, Yamasaki M, Kawamura Y(2013) Evolution of long-period stacking ordered structures on annealing as-cast Mg85Y9Zn6 alloy ingot observed by synchrotron radiation small-angle scattering, ScrMater 68:575-578.

[*24*] Li B, Yan PF, Sui ML, Ma E (2010) Transmission electron microscopy study of stacking faults and their interaction with pyramidal dislocations in deformed Mg,Acta Mater 58:173-179

[25] Hammersley AP, SvenssonSO, Hanfland M, Fitch AN, Häusermann D (1996) Two-Dimensional Detector Software: From Real Detector to Idealised Image or Two-Theta Scan, High Pressure Research14:235-248

[26] http://carine.crystallography.pagespro-orange.fr/

[27] http://www.sigmaplot.com/products/peakfit/peakfit.php

[28] VillarsP, CalvertLD (1985) Pearson´s Handbook of Crystallographic data for intermetallic Phases. American Society for Metals, Metal Park, Ohio 2690

[29] SugamataM, HanawaS, Kaneko J (1997) Structures and mechanical properties of rapidly solidified Mg-Y based alloys, Mater SciEng A 226-228:861-866

[30] AgnewSR, YooMH, Tome CN(2001) Application of texture simulation to understanding mechanical behavior of Mg and solid solution alloys containing Li or Y, Acta Mater49 :4277-4289

[*31*] Grobner J, Kozlov A, Fang XY, Geng J, Nie JF, Schimdt-Fetzer R (2012)Phase equilibria and transformations in ternary Mg-rich Mg–Y–Zn alloys, Acta Mater 60:5948-5962

[*32*] Hagihara K, Sugino Y, Fukusumi Y, Umakoshi Y, Nakano T (2011)Plastic Deformation Behavior of $Mg_{12}ZnY$ LPSO-Phase with 14H-Typed Structure, Mater Trans52:1096-1103

[*33*] Oñorbe E, Garces G, Perez P, Adeva P (2012) Effect of the LPSO volume fraction on the microstructure and mechanical properties of Mg-Y_{2x}-Zn_x alloys, J Mater Sci 47:1085-1093

Figure captions

Figure1. Microstructure ofthe alloys in the as-cast condition. (a) $Mg_{97}Y_2Zn_1$ alloy (OM), (b) $Mg_{97}Y_2Zn_1Gd_{0.5}$ alloy (OM), (c) $Mg_{97}Y_2Zn_1Nd_{0.5}$ alloy (OM) and (d) $Mg_{88}Y_8Zn_4$alloy (SEM).

Figure 2(a-h) Synchrotron diffraction patterns obtained from the 2D detector. (a) $Mg_{97}Y_2Zn_1$,(b) $Mg_{97}Y_2Zn_1Gd_{0.5}$, (c) $Mg_{97}Y_2Zn_1Nd_{0.5}$and (d) $Mg_{88}Y_8Zn_4$ alloys in as-cast condition. (e-h) Detail of the inner ring, which corresponds to the (0003) plane of the LPSO phase.

Figure 3(a-b) Synchrotron diffraction patterns (a) obtained from the 2D detector and (b) as a function of 2θ corresponding to the $Mg_{97}Y_2Zn_1$.

Figure 4. Synchrotron diffraction patterns as a function of 2θ corresponding to the $Mg_{97}Y_2Zn_1$, $Mg_{97}Y_2Zn_1Gd_{0.5}$, $Mg_{97}Y_2Zn_1Nd_{0.5}$ and $Mg_{88}Y_8Zn_4$ alloys. The diffraction patterns of the 18R, 14H and Mg crystal structures were simulated using Carine 3.1. SP designates diffraction reflexes of the stainless steel pan.

Figure 5. (a) Secondary electron image of the microstructure of the as-cast $Mg_{97}Y_2Zn_1Nd_{0.5}$ alloy. (b) Bright field TEM image of the LPSO phase in the as-cast $Mg_{97}Y_2Zn_1Nd_{0.5}$alloy (B=$\langle 11\bar{2}0 \rangle$ and **g**=(0002)). (c) Selected area diffraction pattern of the $Mg_{97}Y_2Zn_1Nd_{0.5}$ alloy in the $\langle 11\bar{2}0 \rangle$ zone axis.

Figure 6. Laboratory DSC scans (heating and cooling) recorded at 10 $Kmin^{-1}$ for the $Mg_{97}Y_2Zn_1$, $Mg_{97}Y_2Zn_1Gd_{0.5}$ and $Mg_{97}Y_2Zn_1Nd_{0.5}$ alloys.

Figure 7(a,b).(a) Synchrotron diffraction patterns at 400 and 560 ºC during heating and at 400 ºC during coolingfor the $Mg_{97}Y_2Zn_1$ alloy. (b) Synchrotron diffraction patterns at 400 ºC during heating, after the endothermic peak during heating and at 400 ºC during coolingfor the $Mg_{97}Y_2Zn_1$,$Mg_{97}Y_2Zn_1Gd_{0.5}$, $Mg_{97}Y_2Zn_1Nd_{0.5}$and $Mg_{97}Y_8Zn_4$alloys.

Figure 8. Synchrotron diffraction patterns for the (a) $Mg_{97}Y_2Zn_1$, (b)$Mg_{97}Y_2Zn_1Gd_{0.5}$ and (c) $Mg_{97}Y_2Zn_1Nd_{0.5}$alloys during cooling from the solidification temperature of the LPSO phase.

Figure 9. Secondary electron image of the $Mg_{97}Y_2Zn_1Nd_{0.5}$alloy after the heating/cooling scan.

Table captions

Table 1. Lattice parameters calculated from diffraction patterns of the magnesium and LPSO phases in the $Mg_{97}Y_2Zn_1$, $Mg_{96.5}Y_2Zn_1Gd_{0.5}$, $Mg_{96.5}Y_2Zn_1Nd_{0.5}$ and$Mg_{88}Y_8Zn_4$ alloys.

Table 2. Composition of the LPSO phase (at.%) in the as-cast state and after the DSC scan in the $Mg_{97}Y_2Zn_1$, $Mg_{97}Y_2Zn_1Gd_{0.5}$ and $Mg_{97}Y_2Zn_1Nd_{0.5}$alloys. The composition of a new Mg-Zn-Y-Nd intermetallic phase (NIP) is also given in the case of $Mg_{97}Y_2Zn_1Nd_{0.5}$.

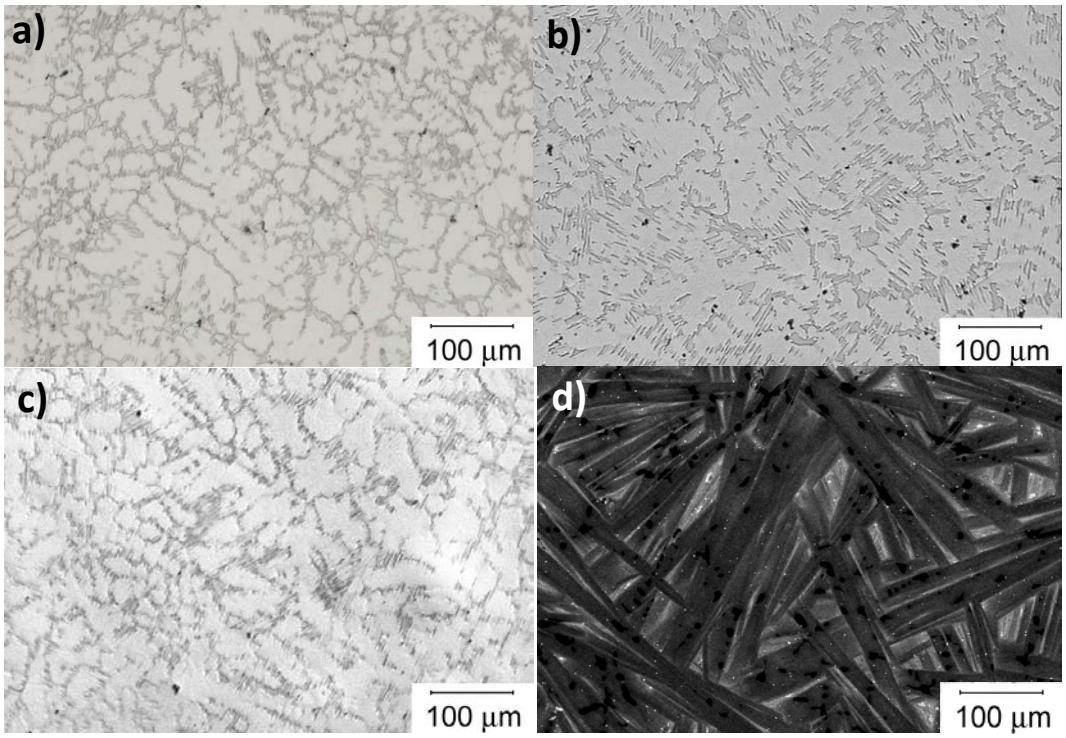

Fig. 1
Microstructure of the alloys in the as-cast condition. a $Mg_{97}Y_2Zn_1$ alloy (OM), b $Mg_{97}Y_2Zn_1Gd_{0.5}$ alloy (OM), c $Mg_{97}Y_2Zn_1Nd_{0.5}$ alloy (OM), and d $Mg_{88}Y_8Zn_4$alloy (SEM)

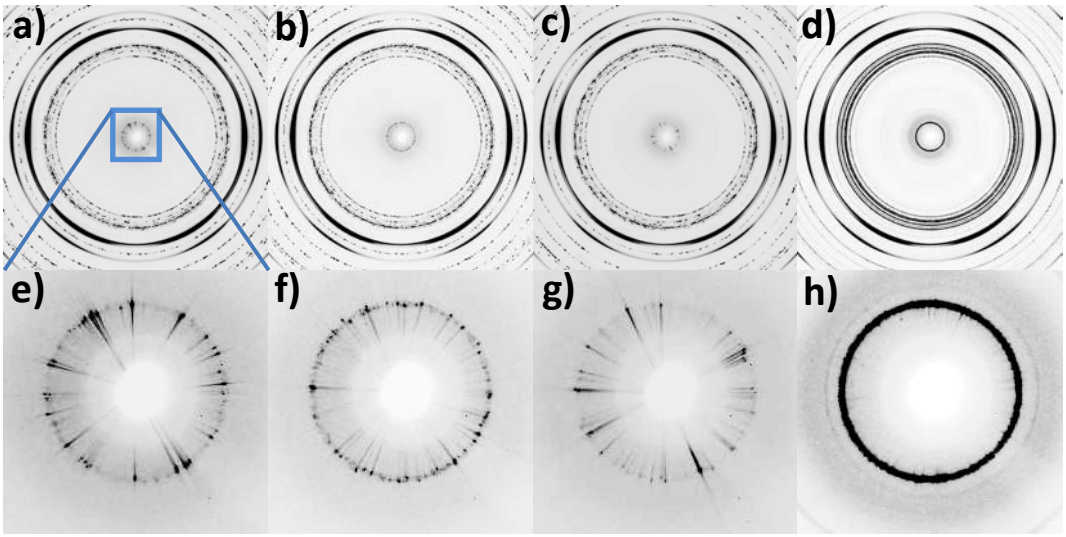

Fig. 2

Synchrotron diffraction patterns obtained from the 2D detector. a $Mg_{97}Y_2Zn_1$, b $Mg_{97}Y_2Zn_1Gd_{0.5}$, c $Mg_{97}Y_2Zn_1Nd_{0.5}$, and d $Mg_{88}Y_8Zn_4$ alloys in as-cast condition. e–h Detail of the inner ring, which corresponds to the (0003) plane of the LPSO phase

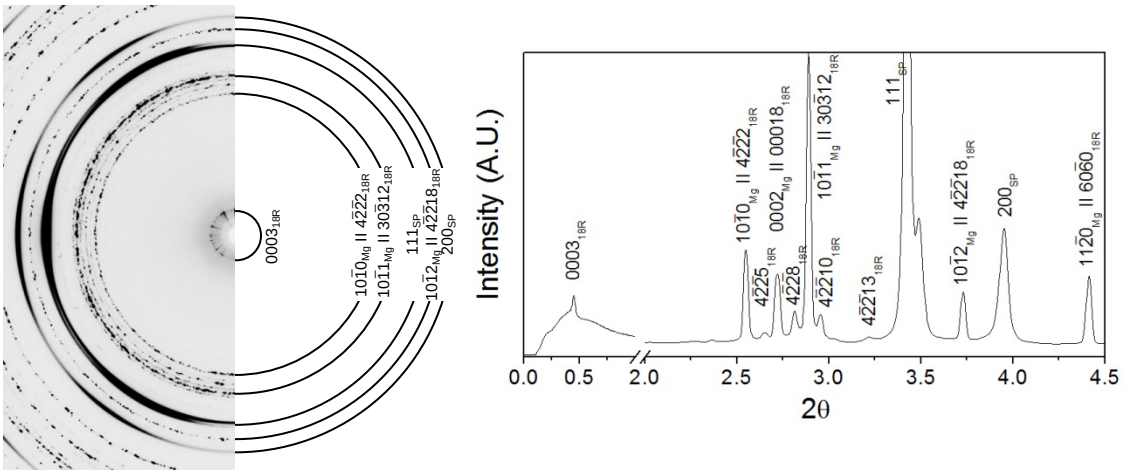

Fig. 3

Synchrotron diffraction patterns: a obtained from the 2D detector, and b as a function of 2θ corresponding to the $Mg_{97}Y_2Zn_1$

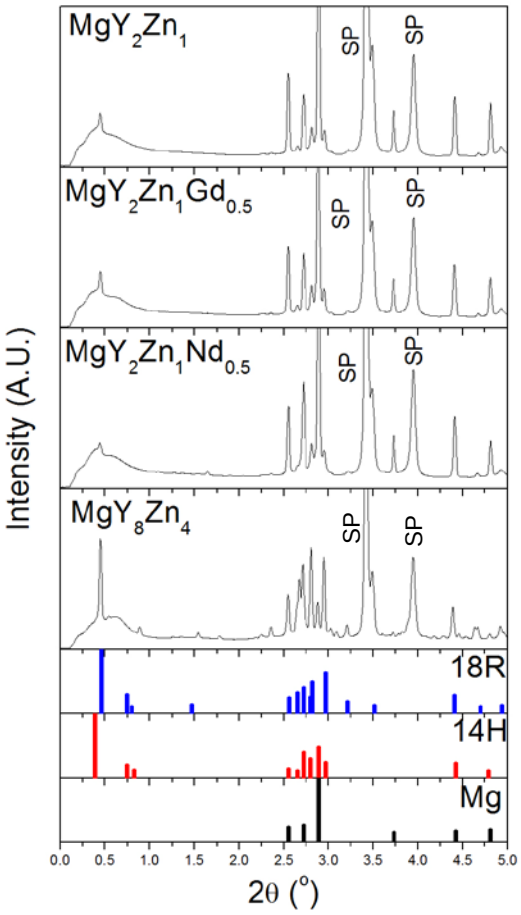

Fig. 4

Synchrotron diffraction patterns as a function of 2θ corresponding to the $Mg_{97}Y_2Zn_1$, $Mg_{97}Y_2Zn_1Gd_{0.5}$, $Mg_{97}Y_2Zn_1Nd_{0.5}$, and $Mg_{88}Y_8Zn_4$ alloys. The diffraction patterns of the 18R, 14H, and Mg crystal structures were simulated using Carine 3.1. SP designates diffraction reflexes of the stainless SP

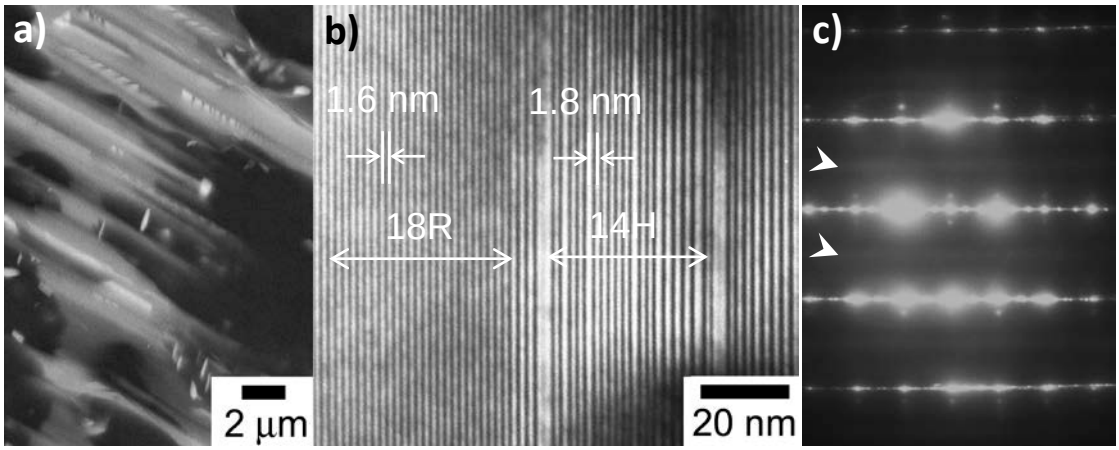

Fig. 5

a Secondary electron image of the microstructure of the as-cast $Mg_{97}Y_2Zn_1Nd_{0.5}$ alloy.

b Bright field TEM image of the LPSO phase in the as-cast $Mg_{97}Y_2Zn_1Nd_{0.5}$ alloy [B = $\langle 112\bar{}0 \rangle$ and g = (0002)].

c Selected area diffraction pattern of the $Mg_{97}Y_2Zn_1Nd_{0.5}$ alloy in the $\langle 112\bar{}0 \rangle$ zone axis

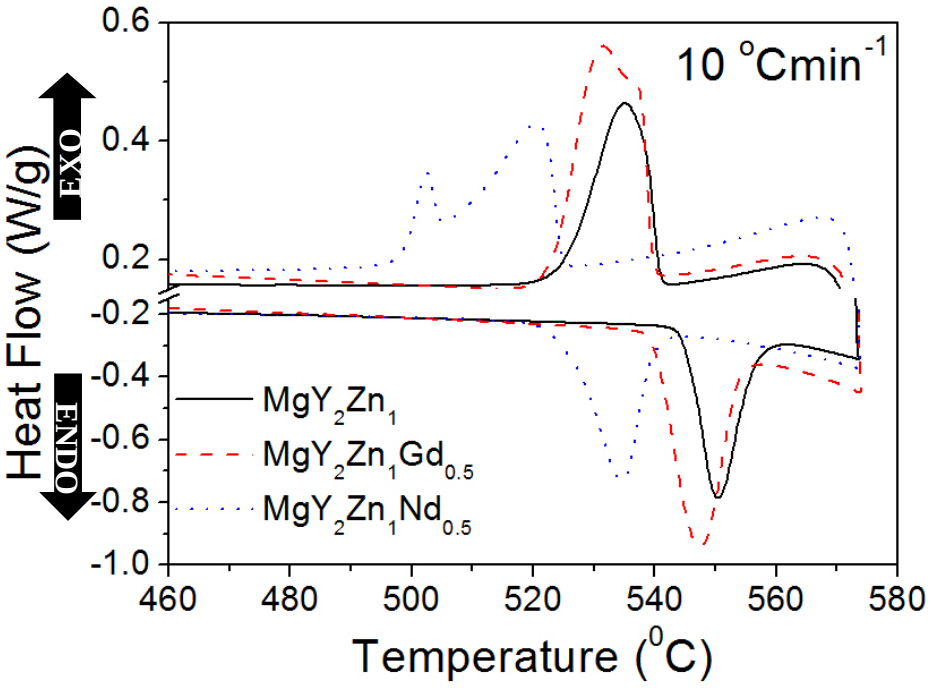

Fig. 6

Laboratory DSC scans (heating and cooling) recorded at 10 K min^{-1} for the $Mg_{97}Y_2Zn_1$, $Mg_{97}Y_2Zn_1Gd_{0.5}$, and $Mg_{97}Y_2Zn_1Nd_{0.5}$ alloys

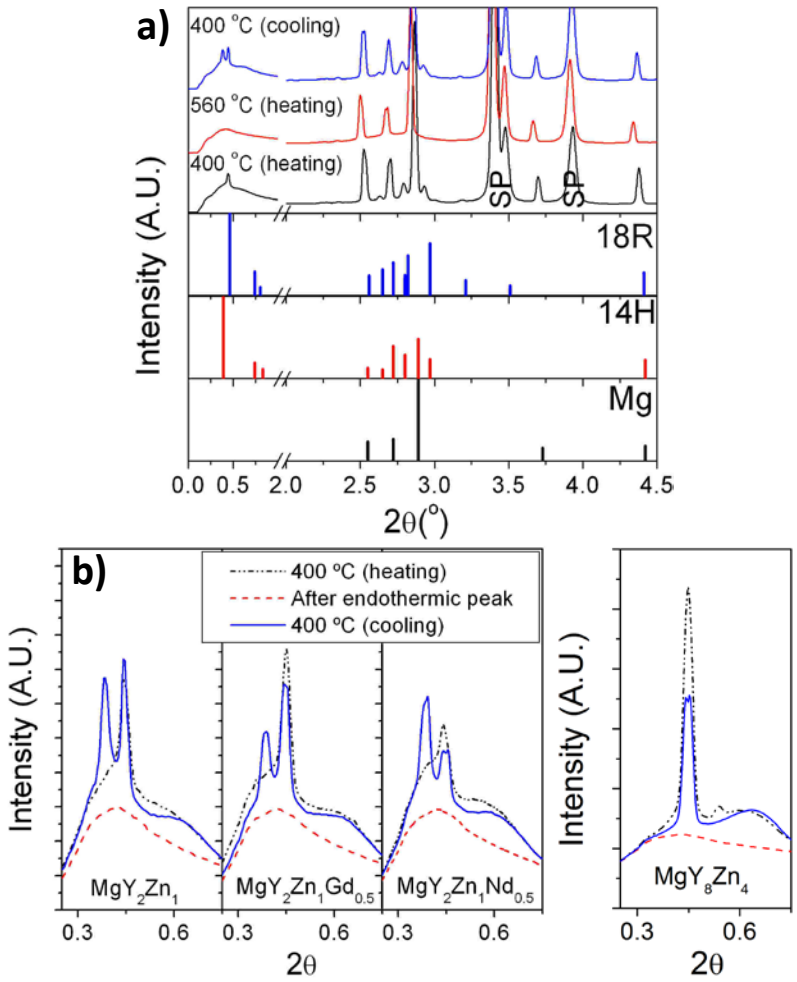

Fig. 7

a Synchrotron diffraction patterns at 400 and 560 °C during heating and at 400 °C during cooling for the $Mg_{97}Y_2Zn_1$ alloy

b Synchrotron diffraction patterns at 400 °C during heating, after the endothermic peak during heating and at 400 °C during cooling for the $Mg_{97}Y_2Zn_1$,$Mg_{97}Y_2Zn_1Gd_{0.5}$, $Mg_{97}Y_2Zn_1Nd_{0.5}$, and $Mg_{97}Y_8Zn_4$ alloys

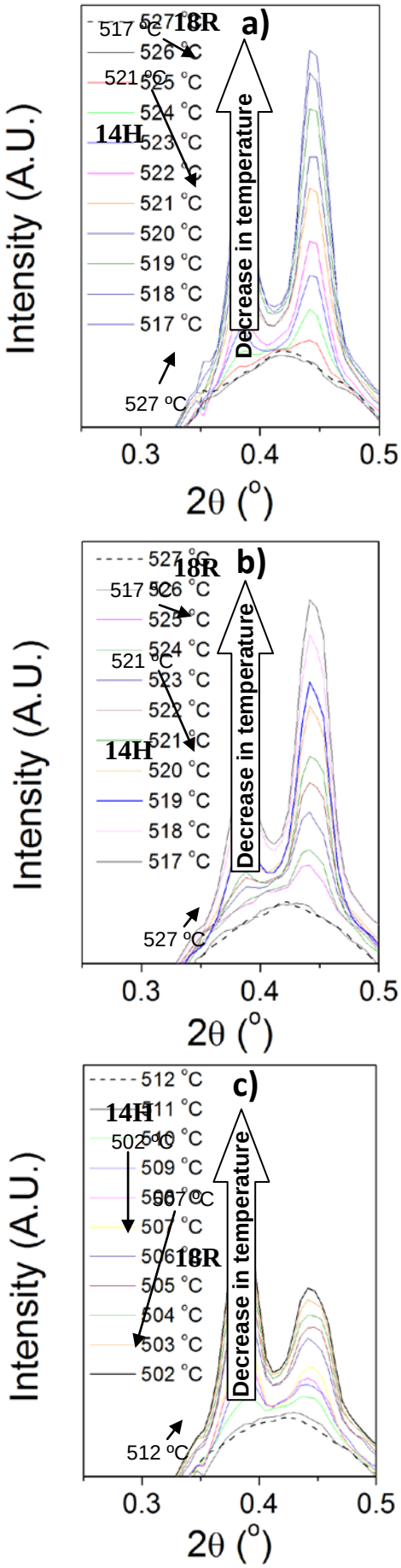

Fig. 8

Synchrotron diffraction patterns for the a $Mg_{97}Y_2Zn_1$, b $Mg_{97}Y_2Zn_1Gd_{0.5}$, and c $Mg_{97}Y_2Zn_1Nd_{0.5}$ alloys during cooling from the solidification temperature of the LPSO phase

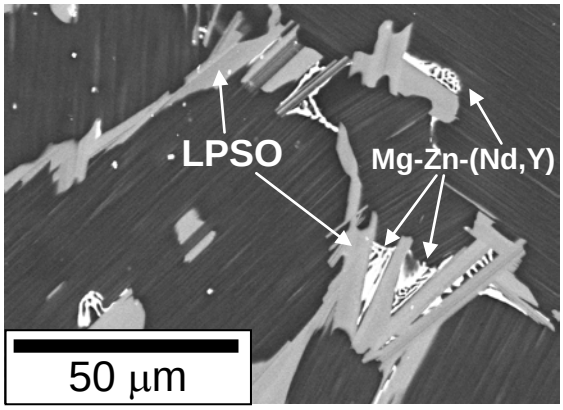

Fig. 9
Secondary electron image of the $Mg_{97}Y_2Zn_1Nd_{0.5}$ alloy after the heating/cooling scan

Table 1

Alloy	LPSO		Mg	
	a(nm)	c (nm)	a (nm)	c (nm)
MgY_8Zn_4	1.111±0.003	4.72±0.07	--	--
MgY_2Zn_1	1.110±0.033	4.74±0.11	0.3221±0.0002	0.52067±0.0015
$MgY_2Zn_1Gd_{0.5}$	1.111±0.020	4.73±0.16	0.3224±0.0002	0.52176±0.0013
$MgY_2Zn_1Nd_{0.5}$	1.111±0.061	4.76±0.29	0.3221±0.0004	0.52013±0.0026

Table 2

Alloy		Mg	Zn	Y	Gd	Nd
MgY_2Zn_1	as-cast	87.2±1.2	5.2±0.2	7.3±0.2	--	--
	after DSC	86.9±1.3	5.5±0.4	7.6±0.3	--	--
$MgY_2Zn_1Gd_{0.5}$	as-cast	88.6±1.2	4.5±0.1	5.5±0.2	1.4±0.1	--
	after DSC	88.5±1.2	4.7±0.1	5.5±0.2	1.3±0.1	--
$MgY_2Zn_1Nd_{0.5}$	as-cast	89.4±1.4	4.4±0.1	4.7±0.3	--	1.5±0.1
	after DSC	88.6±1.5	4.5±0.1	6.1±0.4	--	0.8±0.1
	NIP	61.0±1.0	21.5±1.1	7.4±0.6	--	10.1±0.9